nature synthesis

Article

https://doi.org/10.1038/s44160-023-00331-5

Light-driven biosynthesis of volatile, unstable and photosensitive chemicals from CO_2

Received: 13 September 2022

Accepted: 24 April 2023

Published online: 25 May 2023

Check for updates

Chaofeng Li[1,2], Lijie Yin[1], Jiawei Wang[1,2], Haotian Zheng[1,2] & Jun Ni[1,2]

Directing CO_2 conversion using photoautotrophic microbes offers a promising route to coupling carbon mitigation with petrochemical replacement. However, solar-based biomanufacturing is hampered by inefficient genetic manipulation, narrow product scope and light-induced decomposition. Here we report a spatiotemporally separated modular strategy to realize CO_2-to-molecule conversion by sequentially linking carbon sequestration and cellular catalysis via stable mediator compounds. The carbon fixation rate of the sequestration module was improved by approximately 50% through metabolic network remodelling, while biphasic catalysis, multiple gene editing and high-throughput workflow were applied to the catalysis modules to produce olefins, cinnamaldehyde and curcumin. The catalytic efficiency was notably enhanced by up to 114-fold compared with the monoculture. This modular design approach enables the rapid development of sustainable biorefineries in a plug-and-play fashion, as evidenced by the production of various chemicals at the gram-per-litre level through scaled-up fermentation. This carbon-negative flexible platform notably widens the applicability of light-driven biosynthesis and may boost the bioindustry of CO_2 reduction in a sustainable future.

The valorization of CO_2 is vital for carbon neutrality and the circular economy, yet it remains a huge challenge[1–4]. Light-driven synthetic biology via photosynthetic microorganisms offers a promising route to coupling carbon sequestration with petrochemical replacement[5–7]. However, the molecular tools and automated workflows for the genetic engineering of photosynthetic organisms lag far behind those available for commonly used industrial strains[8,9]. Furthermore, the product spectrum is limited by inherent factors[10,11], for example, essential gas exchange, leading to the ready escape of volatile products, and the light-induced decomposition of photosensitive products (Fig. 1a). Another major concern is the undesirable conversion of target products mediated by endogenous enzymes[12–15], and the elimination of this redundant activity entirely is challenging in underexplored photosynthetic strains. There is currently no solution to these long-standing constraints, and it would be of great importance to develop a universal CO_2 valorization strategy to rapidly synthesize any chemical of interest.

Synthetic phototrophic communities with similar architecture to natural lichens have been used for the distribution of metabolic burden[16,17]. In this consortia design, the modified phototrophs commonly provide sucrose to support the growth of heterotrophs, and the heterotrophs can be flexibly programmed for the photoproduction of target compounds[18,19]. However, they cannot address the limitations mentioned above of light-driven synthetic biology, such as the light-induced decomposition of target products. Inspired by, but different from the one-pot autotroph–heterotroph co-culture, we hypothesized that dividing the CO_2-to-molecule conversion route

[1]State Key Laboratory of Microbial Metabolism, Joint International Research Laboratory of Metabolic and Developmental Sciences, and School of Life Sciences and Biotechnology, Shanghai Jiao Tong University, Shanghai, China. [2]Zhangjiang Institute for Advanced Study, Shanghai Jiao Tong University, Shanghai, China. e-mail: tearroad@sjtu.edu.cn

https://doi.org/10.1038/s44160-023-00331-5

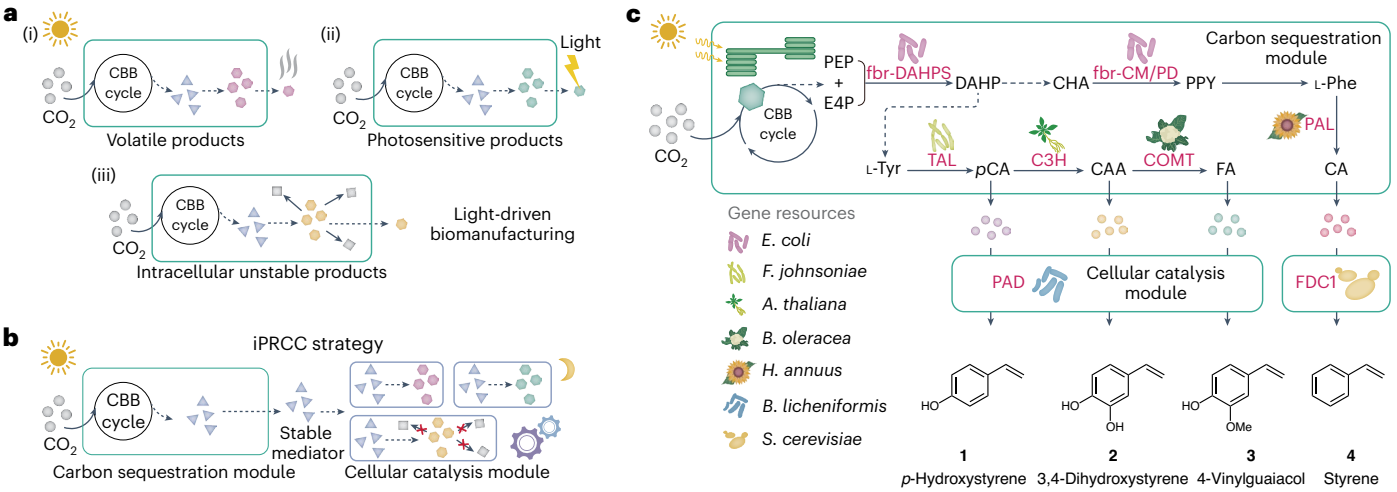

Fig. 1 | Light-driven CO_2 sequestration for biomanufacturing. a, Schematic representation of the three main constraints faced by traditional photosynthetic production: (i) essential gas exchange, leading to the ready escape of volatile products; (ii) light-induced decomposition of photosensitive products; (iii) and the undesirable conversion of target products mediated by endogenous enzymes. **b**, Schematic of the iPRCC strategy, which facilitates CO_2-to-molecule conversion by integrating carbon sequestration and cellular catalysis modules via stable mediator compounds. **c**, iPRCC strategy for the de novo biosynthesis of aromatic α-olefins from CO_2. The carbon sequestration module converts CO_2 into carboxylic acids, which are then catalysed to terminal olefins in the cellular catalysis module. The enzymes from different organisms are labelled in red. Gene resources: *E. coli*, *Flavobacterium johnsoniae*, *Arabidopsis thaliana*, *Brassica oleracea*, *Helianthus annuus*, *Bacillus licheniformis* and *S. cerevisiae*. PEP, phosphoenolpyruvate; E4P, erythrose 4-phosphate; DAHP, 3-deoxy-D-arabino-heptulosonate 7-phosphate; CHA, chorismic acid; PPY, phenylpyruvate; L-Phe, L-phenylalanine; L-Tyr, L-tyrosine; fbr-DAHPS, FBR 3-deoxy-D-arabino-heptulosonate-7-phosphate synthase; fbr-CM/PD, FBR bifunctional chorismate mutase/prephenate dehydratase.

into spatiotemporally separated carbon sequestration and whole-cell catalysis modules may offer new opportunities to solve these problems. In this approach, the carbon sequestration module should first redirect the fixed carbon to stable mediator chemicals, and the subsequent cellular catalysis module should rapidly convert these mediator chemicals to end products. Here, the mediator chemical should not be an easily metabolized chemical or a carbon source that can be used by heterotrophs, and the directional conversion of the intermediate to target chemicals should avoid using the fixed carbon for cell growth. To avoid the inherent limitations of the photosynthetic process, the intermediates should be non-volatile, photostable and unmetabolized by endogenous enzymes. Industrial workhorses such as *Escherichia coli* and *Saccharomyces cerevisiae* have more sophisticated genetic toolkits and maturing high-throughput platforms than photosynthetic microorganisms[20–23]. They are the priority chassis for cellular catalysis modules. The biphasic reaction, light-free catalysis and redundant endogenous enzymes eliminated in the catalysis module may enable the biosynthesis of volatile, photosensitive and unstable intracellular products that are difficult to obtain in photosynthetic mono- or co-cultures. For example, aromatic aldehydes are rapidly converted into alcohols by numerous characterized and uncharacterized endogenous dehydrogenases in photosynthetic microbes, and selecting the correct target genes for knockout is challenging[15,24,25]. The CO_2-to-aromatic aldehyde route can be developed by integrating a whole-cell catalysis module based on reduced aromatic aldehyde reduction (RARE) *E. coli*[15] and a carbon sequestration module. Although this appears to widen the scope of light-driven biosynthesis, no attempts have been made so far to use this modular strategy.

In this Article, we devised a broadly applicable CO_2 valorization strategy, the integration of photosynthesis and resting cellular catalysis (iPRCC), to efficiently convert CO_2 into various value-added chemicals. Multiple gene editing and high-throughput workflow were applied to cellular catalysis modules to produce volatile styrene, intracellular unstable aldehydes and photosensitive molecules. The overall catalytic efficiency of this iPRCC strategy was enhanced up to 114-fold compared with photosynthetic monocultures. We scaled up this system to direct CO_2 conversion at product titres of up to ~2 g l^{-1}, and millions of tonnes of CO_2 could be sequestered for 1 tonne of target chemical. This efficient, carbon-negative route dramatically widens the scope of light-driven biosynthesis and opens up a promising opportunity for a circular economy.

Results

Rewiring cyanobacterial metabolism for mediator production

To evaluate the feasibility of the iPRCC strategy, we chose volatile styrene as the initial target product, a versatile commodity chemical whose global market is expected to reach US$69.9 billion by 2026[26]. However, styrene production based on processes using petroleum feedstock is responsible for over 100 million tons of greenhouse gas emissions each year[27]. We first generated a carbon sequestration module based on a fast-growing photosynthetic microorganism, *Synechococcus elongatus* PCC7942, to channel CO_2 into a stable mediator chemical, cinnamic acid (CA; Fig. 1b). CA was chosen as the mediator chemical for its non-volatility, photostability, secretability and unmetabolizability by endogenous enzymes. The photosynthetically fixed carbon can be easily directed towards the shikimate pathway[28], and CA that derived from this pathway has the potential to achieve high output. In nature, phenylalanine ammonia-lyase (PAL) catalyses the deamination of endogenous phenylalanine to CA[29], and we tested various PAL enzymes by integrating them into the *S. elongatus* genome (Supplementary Fig. 1 and Supplementary Table 1). Although the engineered strains could produce CA directly from CO_2 (Fig. 2a), their initial titres (4.5–8.8 mg l^{-1}) were too low to support further transformation. To redirect fixed carbon into the low-flux shikimate pathway, we used the feedback-inhibition-resistant (FBR) cassette harbouring two FBR enzymes from a previous study as a non-native carbon sink[28]. Strikingly, this strategy increased the CA titre to 156.2 ± 4.1 mg l^{-1} (15.6 mg l^{-1} d^{-1}, strain S116), representing a 25-fold improvement compared with the parent strain S112 (Fig. 2b). Due to metabolic rigidity, metabolic partitioning towards the low-flux shikimate pathway for valuable aromatics is commonly less than 10% in industrial workhorses[30–32]. In contrast, S116 successfully directed more than 30% of the photosynthetically

https://doi.org/10.1038/s44160-023-00331-5

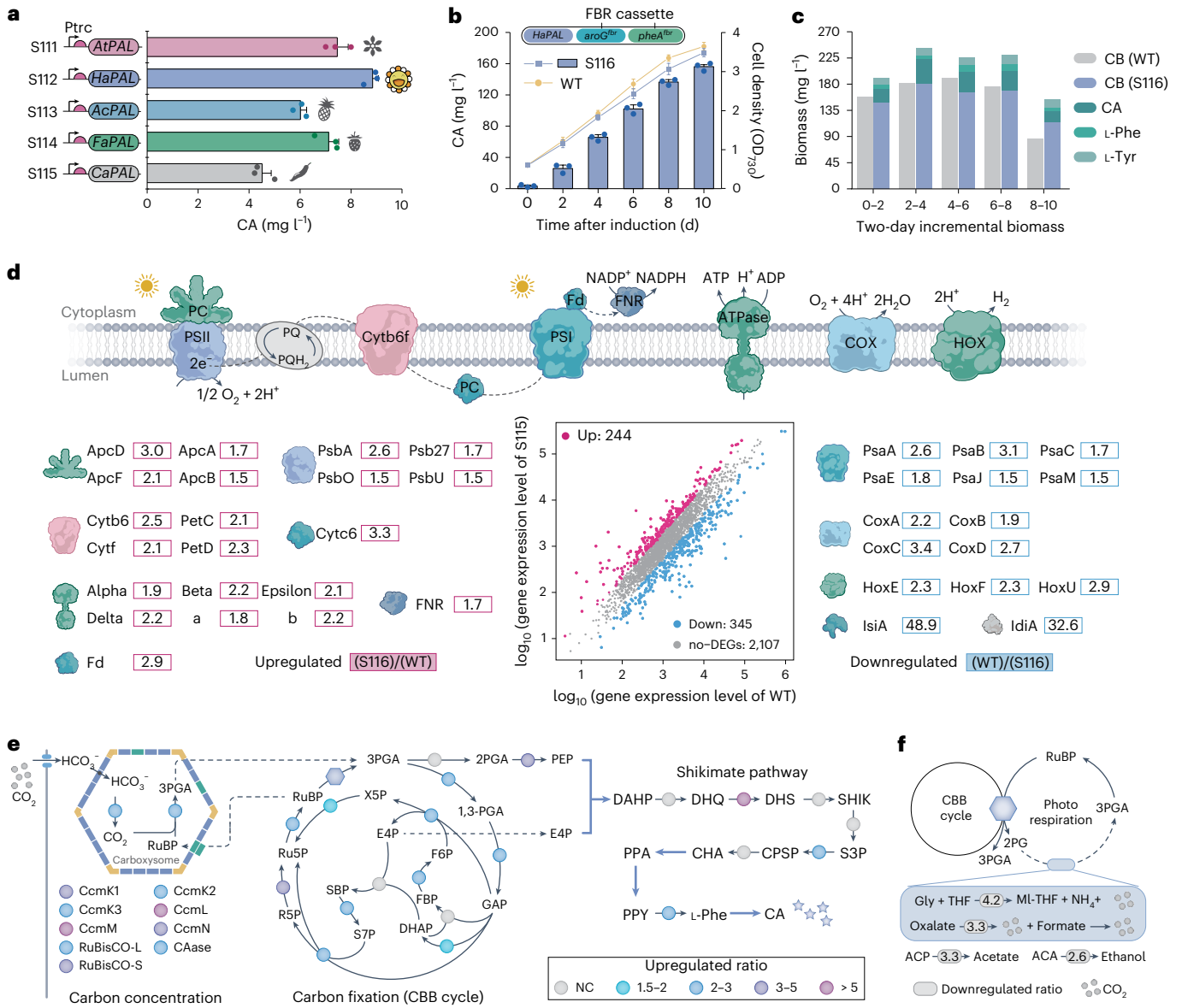

Fig. 2 | Direct photosynthetic CA production. a, CA production by engineered *S. elongatus* strains harbouring *PAL* genes from various sources in 10 days. Ptrc means the trc promoter. *AtPAL*, *HaPAL*, *AcPAL*, *FaPAL*, *CaPAL* indicate the *PAL* genes from *Arabidopsis thaliana*, *Helianthus annuus*, *Ananas comosus*, *Fragaria* × *ananassa*, and *Capsicum annuum*, respectively. **b**, CA production (royal purple columns) and growth curves (royal purple line) of recombinant strain S116 compared with the parent WT strain. Cell growth was measured as the optical density at 730 nm (OD_{730}). In **a** and **b**, values are shown as mean ± s.d. ($n = 3$ biologically independent replicates); dots represent individual data points. **c**, Total biomass production per two-day by WT *S. elongatus* (grey columns) and S116 (royal purple columns) strains. The total biomass is the cell biomass plus the CA and free aromatic amino acids produced. All data represent the mean of $n = 3$ biologically independent samples. **d**, Overview of the regulation pattern of the photosynthetic chain in response to the powerful electron sink in S116. The scatter plot shows the relative transcript levels of all expressed genes in S116 compared with in WT *S. elongatus*. The numbers in red boxes and blue boxes indicate the up-regulated and down-regulated ratios, respectively. The data represent the mean of three biological replicates. ApcA, ApcB, ApcD, and ApcF indicate different allophycocyanin (APC) subunits. PsbA, PsbO, Psb27, and PsbU indicate subunits of photosystem II. Alpha, beta, delta, epsilon, a, and b indicate subunits of ATPase. PsaA, PsaB, PsaC, PsaE, PsaJ, and PsaM indicate subunits of photosystem I. CoxA, CoxB, CoxC, and CoxD indicate subunits of cytochrome c oxidase (COX). HoxE, HoxF, and HoxU indicate subunits of bi-directional hydrogenase complex (HOX). **e**, Unigene transcript abundance changes related to carbon metabolism pathways. The changes in the relative transcript levels for different genes are compared with WT *S. elongatus*. The light-blue arrows indicate the reactions catalysed by heterologous enzymes. **f**, The transcript levels for genes related to photorespiration pathways, acetate kinase and alcohol hydrogenase. CB, cell biomass; PQ, plastoquinone; PQH_2, plastoquinol; PC, plastocyanin; Cytc6, cytochrome *c6*; Fd, ferredoxin; FNR, ferredoxin-nicotinamide adenine dinucleotide phosphate-reductase; Cytb6f, cytochrome b6f complex; Cytb6, cytochrome *b6*; Cytf, cytochrome *f*; PetC, rieske FeS-protein; PetD, subunit IV of Cytb6f; IsiA, iron stress induced protein A; IdiA, iron deficiency induced protein A; CcmK1, CcmK2, CcmK3, CcmL, CcmM, and CcmN indicate subunits of carboxysome; CAase, carbonic anhydrase; RuBisCO-L and RuBisCO-S indicate the subunits of ribulose 1,5-bisphosphate carboxylase/oxygenase (RuBisCO); 3PGA, 3-phosphoglycerate; RuBP, ribulose 1,5-bisphosphate; 1,3-PGA, 1,3-bisphosphoglycerate; GAP, glyceraldehyde 3-phosphate; FBP, fructose 1,6-bisphosphate; DHAP, dihydroxyacetone phosphate; F6P, fructose 6-phosphate; SBP, sedoheptulose 1,7-bisphosphate; S7P, sedoheptulose 7-phosphate; R5P, ribose 5-phosphate; Ru5P, ribulose 5-phosphate; X5P, xylulose 5-phosphate; 2PGA, 2-phosphoglycerate; DHS, 3-dehydroshikimate; SHIK, shikimate; S3P, shikimate 3-phosphate; CPSP, 5-*O*-(1-carboxyvinyl)-3-phosphoshikimate; PPA, prephenate; ACP, acetyl phosphate; ACA, acetaldehyde; Gly, glycine; THF, tetrahydrofolate; Ml-THF, 5,10-methylenetetrahydrofolate.

https://doi.org/10.1038/s44160-023-00331-5

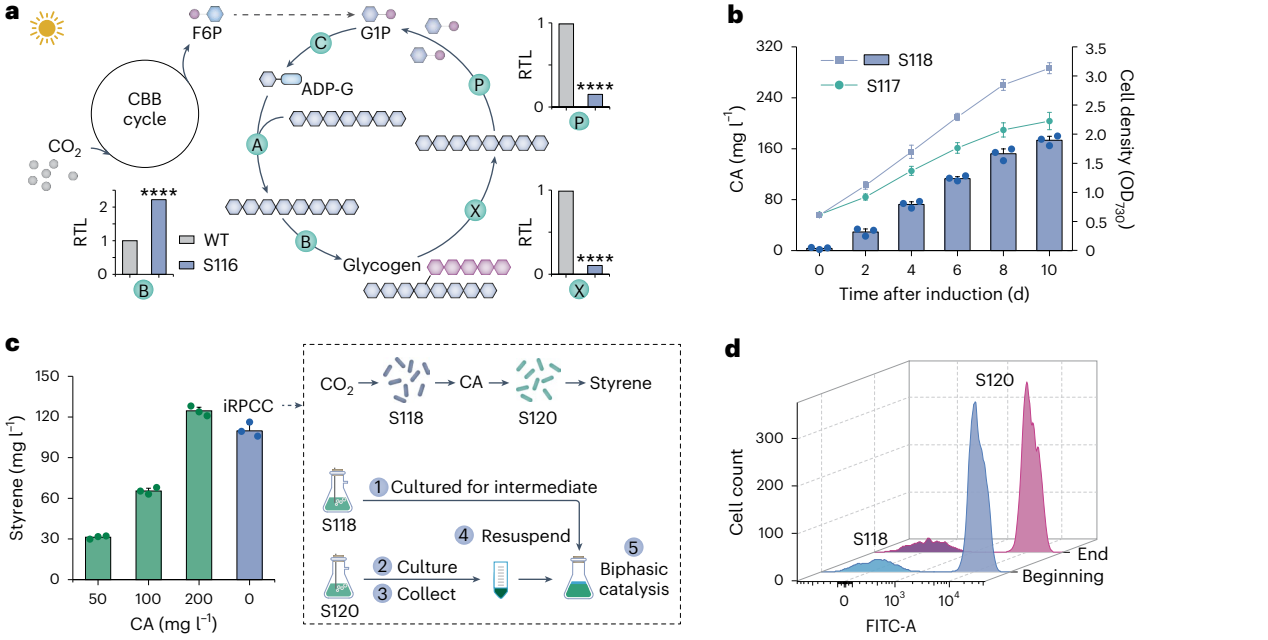

Fig. 3 | Photosynthetic conversion of CO_2 into styrene. a, Schematic of the glycogen metabolism network in cyanobacteria. The green circles indicate the key enzymes in glycogen synthesis. Glucose 1-phosphate (G1P) to ADP-glucose (ADP-G) is catalysed by ADP-glucose pyrophosphorylase (GlgC, C). Glycogen synthase (GlgA, A) transfers glucose monomers to $((1\rightarrow4)$-α-D-glucosyl$)_n$ polymers. Two $((1\rightarrow4)$-α-D-glucosyl$)_n$ polymers are connected by the glycogen branching enzyme (GlgB, B) to generate glycogen. Glycogen debranching enzyme (GlgX, X) hydrolyses the α-1,6-glycosidic bonds and releases the branched glucans. Glycogen phosphorylase (GlgP, P) hydrolyses α-1,4-D-glucan to generate glucose 1-phosphate. The relative transcript levels (RTL) for these key genes are displayed as the ratio of the transcript abundances for S116 compared with WT *S. elongatus*. The data represent the mean of $n = 3$ biologically independent samples. Statistically significant differences in the transcript levels were determined by the two-tailed Student's *t*-test (****$P < 0.0001$). **b**, GlgC knockout promotes CA biosynthesis. CA production (royal purple columns) and growth curves (royal purple line) of recombinant strain S118 under continuous-light culture. The glycogen-deficient strain S117 displayed notable growth retardation (green line). Cell growth was measured as OD_{730}. **c**, Biotransformation of CA to styrene by cellular catalysis module S120 (green columns), and photosynthetic styrene production by the iPRCC strategy (royal purple column). In **b** and **c**, values are shown as mean ± s.d. ($n = 3$ biologically independent replicates); dots represent individual data points. **d**, Flow cytometry analysis of cell count and cell proportion in iPRCC. FITC-A indicates emission intensity at 525 ± 20 nm. For the cell proportion analysis, fwYellow chromoprotein was detected using the fluorescein isothiocyanate (FITC) fluorescence channel to distinguish the two engineered *S. elongatus* strains.

fixed carbon towards the shikimate pathway (Fig. 2c), and the average carbon fixation rate increased by ~50% compared with the wild-type (WT) strain (2.30 versus 1.49 mM OD_{730}^{-1} d^{-1}, OD_{730} means the optical density at 600 nm). Collectively, the non-native carbon sink opened the flux valve of the shikimate pathway in *S. elongatus*, significantly improving the photosynthetic efficiency.

Limited information on how artificial carbon sinks influence inherent photosynthesis, especially photosynthetic machinery and native metabolic sinks, is available[10,33,34]. We conducted a transcriptomic analysis to investigate global changes in S116 and support further engineering (Supplementary Fig. 2). Consistent with most previous studies[10,29,34,35], the main subunits of photosystem II (PSII), electron transport proteins, carboxysomal components and many enzymes in the Calvin–Benson–Bassham (CBB) cycle were upregulated, while several photoprotective mechanisms were sharply downregulated (Fig. 2d,e). In addition, the upregulated PSII subunits and downregulated photosystem I (PSI) subunits coincide with the hypothesis that a lower PSI/PSII ratio may minimize photoinhibition[36]. The photorespiration pathways, acetate kinase and alcohol hydrogenase were downregulated (Fig. 2f), which might minimize the loss of fixed carbon via either released CO_2 or by-products. Based on previous research[37,38], we hypothesized that the enhanced expression of carboxysomal components may contribute to the decreased transcript levels of the photorespiration pathway. The observations described above further proved the enigmatic modulation mechanism in photosynthetic microorganisms that respond to an artificial carbon sink.

Storage polysaccharides are the main natural carbon sinks in *S. elongatus*, and we further examined their synthesis in S116. Although the level of rate-limiting sucrose-phosphate synthase did not change significantly, sucrose production decreased (Supplementary Fig. 3). Surprisingly, GlgC and GlgA, involved in synthesizing glycogen[19,39], were upregulated, and enzymes facilitating the breakdown of glycogen were sharply downregulated (Fig. 3a). Thus, the natural glycogen sink may be enhanced by the reinforced synthesis and suppressed digestion. Indeed, the glycogen content increased by 17 ± 2.3% in S116 (Supplementary Fig. 3c), and this carbon partitioning may compete with the solar-driven production of CA. Therefore, we first constructed a glycogen-deficient mutant to divert the glycogen sink by knocking out the *glgC* gene (S117; Supplementary Fig. 3c). However, the strain displayed notable growth retardation due to the 'carbon sink limitation' (Fig. 3b). The induction of the CA pathway partially rescued the *glgC* null mutant from growth inhibition by rebalancing light-absorption/metabolic sink. The CA titre increased to 173.3 ± 6.3 mg l^{-1} in strain S118 (Fig. 3b), and the specific productivity improved by 23.4 ± 4.5% (55.4 versus 44.9 mg l^{-1} OD_{730}^{-1}).

Interfacing carbon sequestration with cellular catalysis

With a carbon sequestration module (CA-overproducing strain S118) in hand, we further explored different strategies for styrene production. We initially investigated whether a monoculture was suitable for the photosynthetic production of styrene (Supplementary Fig. 4a). Introducing cinnamic acid decarboxylase (FDC1)[40], which catalyses the decarboxylation of the CA, resulted in the production of 4.2 ± 1.1 mg l^{-1} of styrene directly from CO_2 (strain S119; Supplementary Fig. 4b). Notably, prenyl transferase (UbiX) generated the prenylated flavin mononucleotide (prFMN) cofactor necessary for the decarboxylation

https://doi.org/10.1038/s44160-023-00331-5

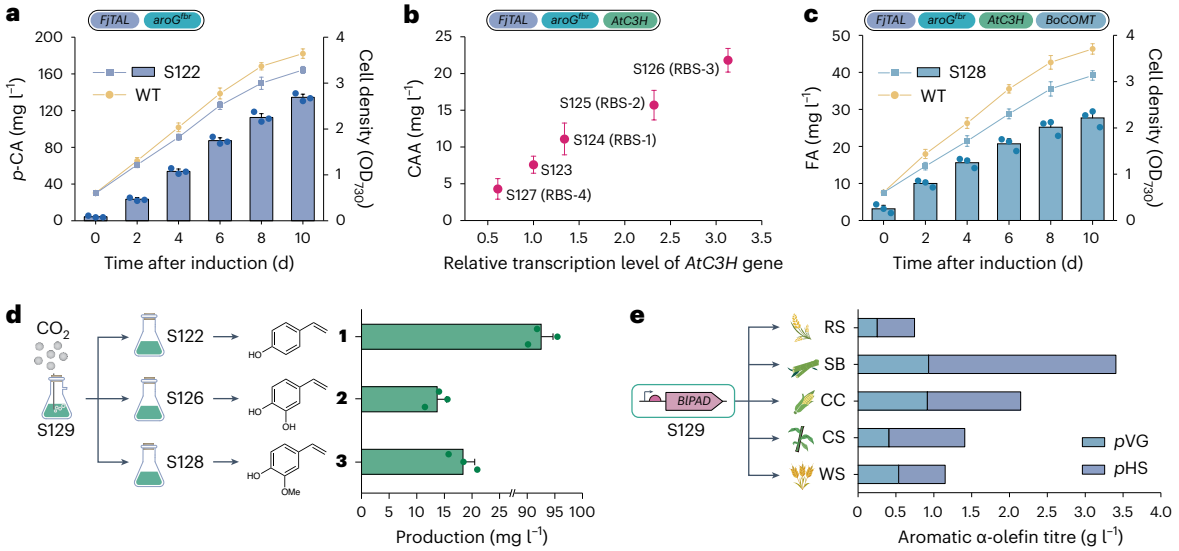

Fig. 4 | Light-driven biosynthesis of other volatile α-olefins. a, Time course of *p*CA production and growth curves of the recombinant strain S122 and the parent WT strain. Cell growth was measured as OD_{730}. Values are shown as mean ± s.d. ($n = 3$ replicates); dots represent individual data points. **b**, CAA titre compared with the relative transcription level of the *AtC3H* gene. The transcription levels of the *AtC3H* gene are given relative to the expression levels of the corresponding *rnpB* gene (the house keeping gene, whose transcription product is the RNA component of RNase P), and the transcription level of the *AtC3H* gene in S123 was set at 1. Four synthetic RBS sequences generated by the RBS calculator were used for *AtC3H* expression. Values are shown as mean ± s.d. ($n = 3$ biologically independent replicates). **c**, FA production (light-blue columns) and growth curves (light-blue lines) of S128 and the parent WT strain under continuous-light culture. Cell growth was measured as OD_{730}. Values are shown as mean ± s.d. ($n = 3$ replicates); dots represent individual data points. **d**, Photosynthetic production of valuable α-olefins **1**–**3** using the iPRCC strategy. The collected cellular catalysis module (S129) was resuspended with the cultures of carbon sequestration modules (S122, S126 or S128). Values are shown as mean ± s.d. ($n = 3$ replicates); dots represent individual data points. **e**, Biosynthesis of olefins *p*VG and *p*HS from several highly abundant lignin-rich agricultural wastes, namely, rice straw (RS), sugarcane bagasse (SB), corn cobs (CC), corn stalk (CS) and wheat straw (WS), over 2 h. The data represent the mean of $n = 3$ biologically independent samples.

activity of FDC1[40], and we speculated that a hypothetical enzyme (accession no. ABB57940.1) in *S. elongatus* may be the prenyl transferase based on its high sequence homology to the UbiX from *Synechocystis* sp. PCC 6803 (Supplementary Fig. 5). As only a limited titre of styrene could be obtained from S119, we speculated that the titre might be underestimated because of the highly volatile nature of styrene and rapid gas exchange during photosynthetic production. Previously, biphasic organic–aqueous systems were used to deal with the evaporation responsible for the significant loss of styrene from *E. coli* liquid culture[41], with the addition of *n*-dodecane allowing the formation of 15.3 ± 1.6 mg l^{-1} of styrene (Supplementary Fig. 4b), representing a 264% improvement. However, the presence of the *n*-dodecane overlay lowered cell growth, and the yield of styrene was far below that of CA production from S118. We concluded that a substantial portion of styrene could still be stripped out by vigorous agitation and constant aeration. Thus, it is difficult to obtain an ideal yield of volatile styrene in a photosynthetic monoculture, regardless of the presence of an organic phase.

Next, we used the iPRCC strategy for styrene production as a proof of concept. To build the resting cellular catalysis module, FDC1 was overexpressed alone in WT *S. elongatus* to form S120. The resting cells of S120 could rapidly catalyse the conversion of CA into styrene with high efficiency in an organic–aqueous biphasic system with 10% (v/v) *n*-dodecane added (Fig. 3c). By interfacing the carbon sequestration module S118 with the resting cellular module S120, 109.8 ± 4.6 mg l^{-1} of styrene was obtained in 10 min (Fig. 3c), representing a 26-fold improvement compared with the monoculture. The production of styrene based on the whole process was about 11 mg l^{-1} d^{-1}, and there was no significant change in the cell densities and ratios during the conversion (Fig. 3d and Supplementary Fig. 6). Thus, we have demonstrated that the biosynthesis of styrene directly from CO_2 by engineered microorganisms can be achieved.

We then implemented this strategy to synthesize other volatile α-olefins directly from CO_2. First, we designed carbon sequestration modules to convert CO_2 into phenolic acids. Tyrosine ammonia-lyase (TAL) was expressed in *S. elongatus* to convert endogenous L-tyrosine into *p*-coumaric acid (*p*CA), with 6.1 ± 0.6 mg l^{-1} of *p*CA being produced by the resulting strain S121 (Supplementary Fig. 7a). After relieving the sole feedback inhibition in the tyrosine biosynthetic pathway by further introducing a FBR enzyme (Supplementary Fig. 8), the engineered strain S122 could produce 134.5 ± 3.4 mg l^{-1} of *p*CA in 10 days, which represents a 22-fold improvement (Fig. 4a). Subsequently, 4-coumarate 3-hydroxylase (C3H) was introduced into S121 (Supplementary Fig. 7b), and the ribosome binding site (RBS) was optimized to boost caffeic acid (CAA) production. Notably, strain S126 with the synthetic RBS-3 sequence increased the CAA titre to 21.8 ± 1.6 mg l^{-1} (Fig. 4b). The next step in the ferulic acid (FA) biosynthesis pathway involves the subsequent methylation of CAA by a caffeate *O*-methyltransferase (COMT), and S128 harbouring this entire synthetic route produced 27.7 ± 1.9 mg l^{-1} of FA from CO_2 (Fig. 4c). Next, the resting cellular catalysis module S129 was constructed by overexpressing phenolic acid decarboxylase (PAD) in *S. elongatus* (Supplementary Fig. 9a). According to the iPRCC strategy, by interfacing resting cellular module S129 with different carbon sequestration modules (S122, S126 or S124), 92.4 ± 2.2 mg l^{-1} of *p*-hydroxystyrene (*p*HS), 13.7 ± 1.7 mg l^{-1} of 3,4-dihydroxystyrene (*p*VC) and 18.4 ± 2.1 mg l^{-1} of *p*-vinylguaiacol (*p*VG) were achieved in 10 min, respectively (Fig. 4d). These compounds are important aromatic monomers for the production of high-performance polymers (Supplementary Table 2). The modularity of the iPRCC strategy also provides various 'plug-and-play' photosynthetic modules. For example, biological lignin valorization is usually limited by techno-economic feasibility[42], and we surmised that the photosynthetic cellular catalyst developed here is more desirable because of the independence of sugar-based feedstocks[43]. The most predominant

https://doi.org/10.1038/s44160-023-00331-5

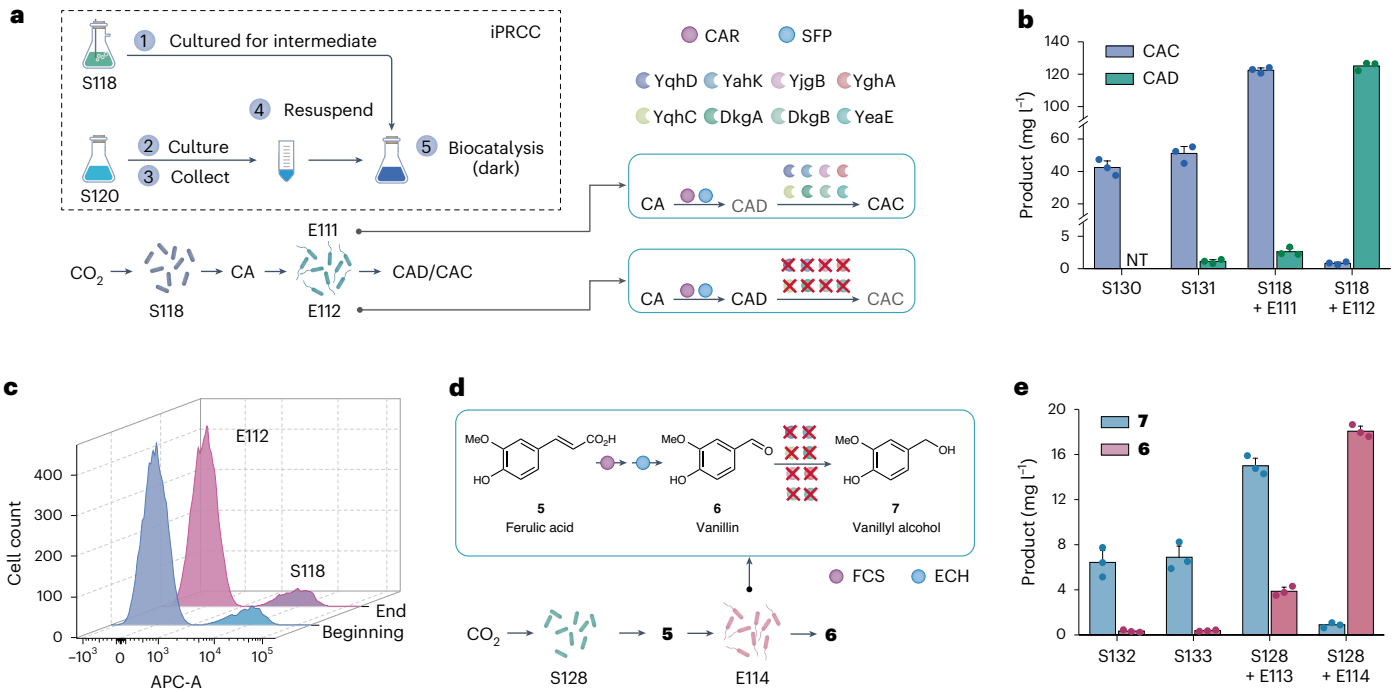

Fig. 5 | Photosynthetic conversion of CO_2 into intracellular unstable products. a, Conceptual schematic of the iPRCC system for photosynthetic CAD production. CAR catalyses the reduction of CA to CAD, and CAD is converted into cinnamic alcohol (CAC) by endogenous ADHs. SFP catalyses the activation of CAR by phosphopantetheinylation. The RARE chassis was constructed by deleting five ADH coding genes (*yqhD*, *yahK*, *yjgB*, *yghA* and *yqhC*) and three AKR coding genes (*dkgA*, *dkgB* and *yeaE*) in *E. coli*. The blocked pathways are marked with red × symbols. **b**, Comparison of the production of CAD and CAC using the monoculture and iPRCC strategy. The mixture of catalysis module and S118 culture was incubated in the dark at 30 °C for 10 min. Values are shown as mean ± s.d. ($n = 3$ replicates); the dots represent individual data points. **c**, Flow cytometry analysis of cell count and cell proportion for iPRCC. For the cell proportion analysis, the endogenous APC protein of *S. elongatus* was detected using the APC fluorescence channel in iPRCC production to distinguish the *S. elongatus* and *E. coli* strains. APC-A indicates emission intensity at 660 ± 10 nm. **d**, Schematic of the iPRCC system for photosynthetic vanillin production. FCS, feruloyl-CoA synthetase; ECH, enoyl-CoA hydratase/aldolase. **e**, Comparison of the production of vanillin and vanillyl alcohol using the monoculture and iPRCC strategy. Values are shown as mean ± s.d. ($n = 3$ biologically independent replicates); the dots represent individual data points.

monomers, *p*CA and FA[24], can be released in different ratios after alkaline hydrolysis of lignin-rich agricultural waste (Supplementary Fig. 9b). Resting module S129 serves as a photosynthetic biocatalyst for the simultaneous conversion of these hydrolysates into a maximum of 2,475.2 ± 4.1 mg l^{-1} of *p*HS and 931.5 ± 5.2 mg l^{-1} of *p*VG (Fig. 4e). These results indicate the feasibility of the value-added use of waste resources by the resting cellular catalysis module.

Multidimensional engineering for efficiency improvement

Light-driven CO_2 conversion using photoautotrophic microorganisms is hampered by redundant endogenous enzymes[12,13]. Thus, solar-dependent biomanufacturing of unstable intracellular products (for example, aromatic aldehydes) remains an ongoing challenge. To demonstrate the potential of our iPRCC strategy, we attempted to convert CO_2 into cinnamaldehyde. We initially extended the CA synthesis pathway by introducing carboxylic acid reductase (CAR) and phosphopantetheinyl transferase (SFP) into the CA-overproducing strain[44]. However, no cinnamaldehyde was detected in the engineered strain S130, and, therefore, we surmised that cinnamaldehyde was rapidly converted by endogenous alcohol dehydrogenases (ADHs). Next, a potential ADH (*synpcc7942_0459*) was deleted, and the resulting strain S131 produced trace amounts of cinnamaldehyde (~1.1 mg l^{-1}; Supplementary Fig. 10a). Aromatic aldehydes are vulnerable to metabolism by more than ten endogenous ADHs and aldo-keto reductases (AKRs) in many microorganisms, and selecting and knocking out the correct target genes to entirely eliminate redundant activity is challenging in underexplored photosynthetic strains[15,25]. Using the iPRCC strategy, we constructed a resting cellular catalysis module that efficiently converts CA into cinnamaldehyde (CAD). Here, *E. coli* was the primary chassis for sophisticated genetic tools and maturing high-throughput workflows, and it was easily manipulated to eliminate redundant endogenous enzymes[15,21]. We constructed a RARE chassis using the clustered regularly interspaced short palindromic repeats (CRISPR)–Cas9 system to delete five ADH coding genes and three AKR coding genes in *E. coli*, and CAR and SFP were then overexpressed (Fig. 5a). Subsequently, 125.1 ± 2.0 mg l^{-1} of CAD was obtained directly from CO_2 by interfacing carbon sequestration module S118 with catalysis module E112 (Fig. 5b), representing a more than 114-fold improvement compared with the monoculture. No significant change in the cell densities and ratios was observed during bioconversion over 10 min (Fig. 5c and Supplementary Fig. 11). Vanillin, a widely used aromatic aldehyde[24], could also be produced from CO_2 using the iPRCC strategy (Fig. 5d). To achieve this, we paired the carbon sequestration module S128 with a downstream heterogeneous catalysis module E114 to produce 18.1 ± 0.4 mg l^{-1} of vanillin in 10 min, representing a 45-fold improvement compared with the monoculture (S133, 0.4 mg l^{-1}; Fig. 5e and Supplementary Fig. 10b).

In addition to volatile and intracellular unstable products, we further widened the scope of light-driven biosynthesis by generating photosensitive products that seem unlikely to be obtained by solar-dependent biomanufacturing due to light-induced decomposition. We synthesized photosensitive curcumin directly from CO_2 by extending the FA pathway by introducing 4-coumaroyl coenzyme A (CoA) ligase (4CL) and curcuminoid synthase (CUS)[45]. As the engineered strain S134 produced only a tiny quantity (<1 mg l^{-1}) of curcumin (Supplementary Fig. 10d), we speculated that this photosensitive compound decomposed during illumination of the culture. Using the iPRCC strategy, the

https://doi.org/10.1038/s44160-023-00331-5

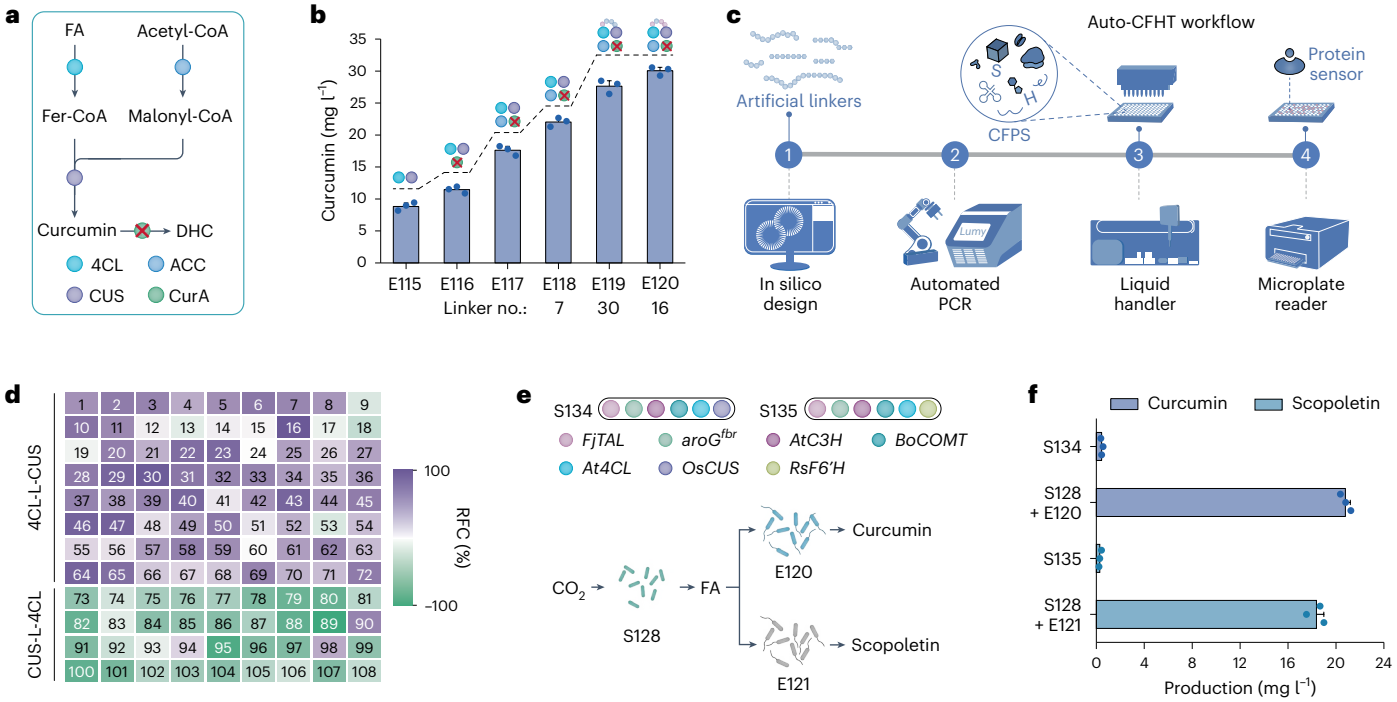

Fig. 6 | Photosynthetic conversion of CO_2 into photosensitive products. **a**, Overview of the metabolic pathway for the formation of curcumin. Fer-CoA, feruloyl-CoA. DHC, dihydrocurcumin. **b**, Curcumin production over 3 h from the resting cellular catalysis module by stepwise metabolic engineering. Values are shown as mean ± s.d. ($n = 3$ biologically independent replicates); the dots represent individual data points. **c**, Practical overview of LumyBio's auto-CFHT workflow. The workflow consists of four parts: in silico design, automated PCR, cell-free prototyping and fluorescence detection. CFPS, cell-free protein synthesis. **d**, Heatmap showing the relative fluorescence change (RFC) based on different fusion proteins of 4CL and CUS. The purple and green colours indicate a higher and lower fluorescence intensity compared with the free proteins (mean of three biological replicates), respectively. The highest fluorescence intensity was set at 100%, and the lowest intensity was set at −100%. 4CL-L-CUS (72 fusion proteins) represents the carboxy terminus of 4CL coupled to the amino terminus of CUS, and CUS-L-4CL represents the C terminus of CUS coupled to the N terminus of 4CL. The numbers in the boxes represent different linkers, and the corresponding amino acid sequences of these linkers are shown in Supplementary Table 3. **e**, Schematic of the iPRCC system for the photosynthetic production of curcumin and scopoletin. Feruloyl-CoA 6′-hydroxylase (F6′H) was encoded by *RsF6′H*. **f**, Comparison of the production of curcumin and scopoletin using the monoculture and iPRCC strategy. The mixture of catalysis module and S128 culture was incubated in the dark at 30 °C for 2 h. Values are shown as mean ± s.d. ($n = 3$ biologically independent replicates); the dots represent individual data points.

CO_2-to-curcumin route can be divided into a CO_2-to-FA sequestration module (light module) and an FA-to-curcumin catalysis module (dark module) to avoid light-induced decomposition (Fig. 6a). Because S128 can serve as a carbon sequestration module, a catalysis module that efficiently converts FA into curcumin should be constructed to test our hypothesis. First, the introduction of 4CL and CUS into *E. coli* (strain E115) resulted in the production of 8.8 ± 0.5 mg l^{-1} of curcumin. Then, the endogenous curcumin reductase (CurA) was knocked out (strain E116), which produced 11.5 ± 0.4 mg l^{-1} of curcumin (Fig. 6b). Furthermore, acetyl-CoA carboxylase (ACC) was overexpressed to improve intracellular malonyl-CoA levels, which enabled a curcumin titre of 17.6 ± 0.6 mg l^{-1} (strain E117). Next, to further enhance FA bioconversion, the unnatural fusion of 4CL and CUS was engineered to channel substrates into sequential reactions. In this approach, it is critical to design and optimize the interpeptide linkers[46]. By combining advanced liquid-handling technologies and artificial protein biosensors, we explored an automated cell-free high-throughput (auto-CFHT) workflow to accelerate linker optimization (Fig. 6c). We screened a library of hundreds of linkers (Supplementary Table 3), and the flexible linker 16 (L-16) showed the best performance (Fig. 6d). To our knowledge, this represents the highest number of linkers tested for biosynthesis in vitro. Intriguingly, the best fusion protein has better spatial proximity (shorter interdistance and more face-to-face channels)[47], which may explain why the catalytic efficiency was higher (Supplementary Fig. 12). Replacing 4CL and CUS with fusion proteins enhanced the curcumin titre to 30.1 ± 0.5 mg l^{-1} (E120, with L-16), representing a 71% improvement (Fig. 6b). Here, the results of in vivo and in vitro experiments showed a positive correlation (Fig. 6b,d and Supplementary Fig. 12e). Subsequently, by interfacing carbon sequestration module S128 with catalysis module E120, 20.8 mg l^{-1} of curcumin was obtained directly from CO_2 (Fig. 6e,f), representing a 46-fold improvement compared with the monoculture. No significant change in the cell densities and ratios was observed during conversion for 2 h (Supplementary Fig. 11d). Another photosensitive compound, scopoletin, could also be produced from CO_2. Combining carbon sequestration module S128 with catalysis module E121 produced 18.4 ± 0.6 mg l^{-1} of scopoletin, representing a 61-fold improvement compared with the monoculture (S135, 0.3 mg l^{-1}; Fig. 6f). Our results reveal that the carbon-negative flexible platform based on the iPRCC strategy dramatically expands the scope of light-driven biosynthesis.

Expanding the carbon-negative flexible platform

The iPRCC strategy enables CO_2-to-molecule conversion by modular design, and the carbon sequestration modules developed here could convert CO_2 into phenolic acids, the gatekeeper molecules for polyphenol biosynthesis[48]. Thus, coupling these carbon sequestration modules with other autotrophic/heterotrophic catalysis modules that harbour complementary pathways could yield a range of

https://doi.org/10.1038/s44160-023-00331-5

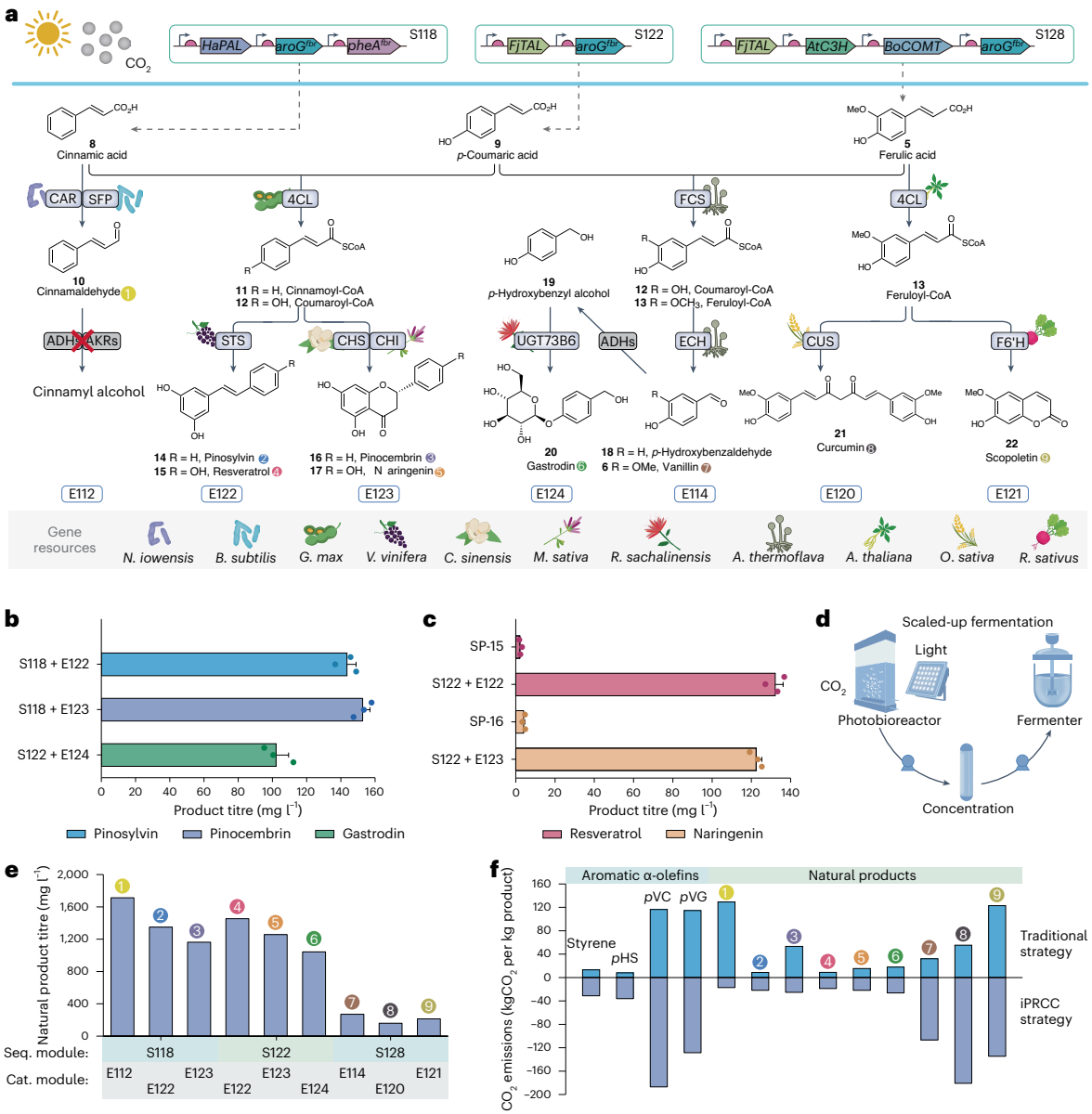

Fig. 7 | Carbon-negative production of various valuable chemicals by the iPRCC strategy. a, Overview of the metabolic pathway towards the production of natural compounds based on the iPRCC strategy. The final natural compounds are labelled with numbers in coloured circles, which can be used to identify the natural products in **e** and **f**. Gene resources: *Nocardia iowensis*, *Bacillus subtilis*, *Glycine max*, *Vitis vinifera*, *Camellia sinensis*, *Medicago sativa*, *Rhodiola sachalinensis*, *Amycolatopsis thermoflava*, *A. thaliana*, *Oryza sativa* and *Raphanus sativus*. STS, stilbene synthase; CHS, chalcone synthase; CHI, chalcone isomerase; UGT73B6, glycosyltransferase. **b**, Photosynthetic production of pinosylvin, pinocembrin and gastrodin by the iPRCC strategy. The mixture of catalysis module and S118 or S122 culture was incubated in the dark at 30 °C for 2 h. **c**, Comparison of the production of resveratrol and naringenin using the monoculture and iPRCC strategy. In **b** and **c**, the values and error bars represent means and standard deviations of experiments performed in triplicate; the coloured circles represent individual data points. **d**, Schematic of the scaled-up fermentation process. The carbon sequestration modules were cultured in a photobioreactor. Then, cultures of *S. elongatus* were concentrated in a rotary vacuum evaporator and transferred to a 1.5-l fermenter with appropriate cellular catalysis modules. **e**, Fermentation performance of iPRCC-based systems in a 12-l photobioreactor coupled with a 1.5-l fermenter. The sequestration (Seq.) and catalysis (Cat.) modules are specified below the chart. **f**, Comparison of the CO_2 emissions from traditional sugar-based production routes and iPRCC-based routes. Positive and negative values indicate CO_2 emission and CO_2 consumption, respectively. Traditional routes result in CO_2 emission (blue columns), while iPRCC-based routes avoid CO_2 emission (royal purple columns), effectively fixing carbon into the products.

valuable natural products (Fig. 7a). To validate this concept, we constructed three new catalytic modules (E122, E123 and E124) for the efficient conversion of phenolic acids, in addition to the catalytic modules developed for CAD, vanillin, curcumin and scopoletin production (Supplementary Fig. 13). Interfacing the carbon sequestration modules S118 or S122 with catalysis modules E122, E123 and E124 gave 143.6 ± 5.3 mg l^{-1} of pinosylvin, 152.7 ± 4.3 mg l^{-1} of pinocembrin, 102.1 ± 7.3 mg l^{-1} of gastrodin, 132.1 ± 4.0 mg l^{-1} of resveratrol and 122.5 ± 2.9 mg l^{-1} of naringenin directly from CO_2 (Fig. 7b,c). Compared with the results of previous research on monocultures (constructs SP-15 and SP-16 from *S. elongatus*, Supplementary Fig. 13d)[49], the titres of resveratrol and naringenin were dramatically enhanced 63- and 31-fold, respectively, using the iPRCC strategy (Fig. 7c). It is important to note that while our approach can be readily

adapted to a wide range of commodity chemicals, there is still room for improvement.

Next, we sought to ascertain the applicability of the iPRCC process to scaled-up fermentation. The carbon sequestration modules were cultured in a 12-l photobioreactor, and phenolic acid production was at least 120% higher (Supplementary Fig. 14). By interfacing the photobioreactor with a 1.5-l fermenter (Fig. 7d), up to 1.7 g l^{-1} of natural products could be successfully achieved (Fig. 7e). The productivity of this process is close to that of some heterotrophic organisms, and the highest titre obtained here is even higher than that of many heterotrophic microorganisms using carbohydrates (Supplementary Table 4 and Supplementary Fig. 15). A key benefit of solar-based biomanufacturing is its negative carbon footprint. Not taking into account carbon absorption during plant growth, traditional biomanufacturing processes depend on sugar-based feedstocks and are associated with net-positive CO_2 emissions, contributing to global warming[43,50], for instance, at least 11.9 $kgCO_2$ equivalents ($kgCO_2e$) per kg of produced styrene and 31.4 $kgCO_2e$ kg^{-1} of produced vanillin. Conversely, solar-based biomanufacturing effectively locks carbon into the products. We estimated that 17.2–180.9 tCO_2 can be sequestered for 1 tonne of target product (a negative carbon footprint of −17.2 to −180.9 $kgCO_2e$ kg^{-1} of products) by using the iPRCC strategy (Fig. 7f). Accordingly, this easy-to-develop and flexible biotechnique has unique advantages for carbon-negative manufacturing and the circular economy.

Discussion and conclusion

Climate change is a pervasive threat to biodiversity, the economy and the overall quality of life. Light-driven CO_2 valorization using synthetic biology promises to simultaneously alleviate climate warming and achieve sustainable manufacturing[5–7]. However, the molecular tools and automated workflows available for genetic engineering in photosynthetic organisms lag far behind those available for the commonly used heterotrophic workhorses[9]. Nowadays, synthetic phototrophic communities have become increasingly important and attractive for their great potential in the circular bioeconomy[16–19,51–54]. They artfully break up the CO_2-to-molecule conversion route into carbon sequestration and biosynthesis modules for the division of metabolic labour[18,19]. A number of phototrophic communities containing cyanobacteria and different heterotrophic partners have been successfully established for chemical production directly from CO_2 (Supplementary Table 5). However, the one-pot autotroph–heterotroph co-culture does not seem to address the long-standing constraints of light-driven biosynthesis, such as the light-induced decomposition of target products. In this study, we have developed a viable and potentially general CO_2 valorization platform based on a modular strategy called iPRCC. For the carbon sequestration module, the CO_2 fixation rate was notably improved by metabolic network remodelling, and an ingenious self-modulation mechanism in the photosynthetic system has been proposed. Benefiting from the sophisticated genetic tools available for *E. coli*, we implemented substantial strain engineering to rapidly generate and optimize a series of resting cellular catalysis modules. In particular, we adopted the auto-CFHT workflow to accelerate linker optimization markedly. Unlike the commonly used automated high-throughput biofoundry pipelines, which require numerous pieces of equipment[55], only an integrated fluent automation workstation is sufficient for auto-CFHT, which can also be used for pathway prototyping and cell-free biomanufacturing. The iPRCC strategy provides a roadmap for widening the product scope of light-driven biosynthesis, and more than ten valuable molecules have been manufactured sustainably from CO_2 (Supplementary Fig. 16). Remarkably, many of the natural compounds produced here are historically challenging to synthesize, while they are widely used as active ingredients in medicine. For example, scopoletin has considerable potential for combating the COVID-19 pandemic[56]. Compared with monocultures, the titres of the products obtained by the iPRCC strategy were improved by up to two orders of magnitude, and gram-per-litre levels were achieved through scaled-up fermentation, demonstrating the superiority of the iPRCC system.

The choice of mediator chemicals is vital for establishing an iPRCC-based carbon-negative platform, and there are several selection criteria that need to be considered: (1) high photostability and low volatility, (2) resistance to endogenous enzymes, (3) not an available carbon source, (4) easily secreted into the medium, (5) derived from high-flux pathways and (6) preferably metabolite nodes with strong expansibility. In this study, we chose phenolic acids, the gatekeepers of the phenylpropanoid biosynthesis pathway, as mediator chemicals. Thus, an enormous array of natural products could be obtained by simply replacing the catalytic modules with newly constructed or already existing modules. In addition, many precursor substances, such as mevalonate and lactate, are suitable mediators of the carbon-negative biosynthesis of terpenes, degradable plastics and other valuable compounds[57,58]. It is important to note that the catalysis modules we used here were mainly based on *E. coli* for convenient engineering. However, the culture of heterotrophic microorganisms requires a specific organic carbon and nitrogen source. This nutritional requirement can be solved in two ways: (1) by using photosynthetic catalysis modules as an alternative to that used for the biosynthesis of olefins and (2) by converting the biomass from the carbon sequestration module into carbohydrate-rich and organic nitrogen-rich feedstock for feeding the catalysis modules. Also, the alginate encapsulation technology is expected to stabilize and recycle the catalysis modules[59]. Although we used a photobioreactor for scaled-up fermentation, an outdoor pond system should further reduce large-scale manufacturing costs. A recent study has suggested that scaling up the semi-continuous cultivation of *S. elongatus* in an outdoor pond system could bring the minimum biomass price down to US$281 per tonne (ref. 60). Thus, our carbon-negative flexible platform may enable economically competitive applications in broader industries.

In conclusion, the iPRCC strategy provides a general carbon-negative platform for converting CO_2 into a wide range of commodity chemicals. In addition, the dual-mode process can be easily adapted to other target products because of its compatibility with existing microbial cell factories. This may facilitate the further development of light-driven synthetic biology. The other key benefit offered by light-driven biomanufacturing is its negative carbon footprint, and using CO_2 instead of sugars as the initial feedstock decouples biosynthesis from commodity prices. For example, by a back-of-the-envelope calculation, at least 100 tonnes of CO_2 can be sequestered for 1 tonne of vanillin. Additionally, the rising carbon tax (for example, Can$20 per tonne increasing to Can$170 per tonne by 2030 in Canada)[61] may facilitate this carbon-negative manufacturing. We hope this broadly applicable platform will boost the bioindustry of CO_2 reduction for a more sustainable future.

Methods

Transformation of *S. elongatus*

Plasmids were naturally transformed into *S. elongatus* as previously described.[49] Strains were grown to an OD_{730} of about 0.6, and then 2 μg of plasmid DNA was added to 500 μl cultures. The strains were spread on BG-11 plates supplemented with spectinomycin (20 μg ml^{-1}) after 12 h of culture in the dark. All inserted genes were amplified by PCR and sequencing to confirm that they were integrated into the correct site.

Carbon partitioning and carbon emission analysis

S. elongatus cells were collected and dried at 80 °C for 18 h and then measured gravimetrically; the dry cell weight was regarded as the cell biomass. Carbon partitioning (P_{CP}) is equal to the increased carbon of the products (CA, free L-Phe and free L-Tyr) divided by the sum of the increased carbon: $P_{CP} = (W_{CA} + W_{Phe} + W_{Tyr})/(W_{CB} \times C_C + W_{CA} + W_{Phe} + W_{Tyr}) \times 100\%$, where W_{CB} is the increased cell biomass, C_C is the carbon content of the cell biomass (51.34%)[29], and W_{CA}, W_{Phe} and W_{Tyr} are the increased

carbon in CA, L-Phe and L-Tyr, respectively. The average carbon fixation rate, R_{CO_2} R, was calculated from the sum of the increased carbon and specific growth rate: $R_{CO_2} = (W_{CB} \times C_C + W_{CA} + W_{Phe} + W_{Tyr})/P_{OD_{730}}/T$, where $P_{OD_{730}}$ is the average growth of *S. elongatus* per day and T is the time (day). The amount of carbon in the products was calculated from the product titres (mmol l^{-1}), multiplied by 9 (the number of molecules of CO_2 fixed per molecule of CA, L-Phe or L-Tyr produced). The increased carbon was calculated by taking the carbon measured at one time point and subtracting 99% of the carbon measured at the previous time point (1% of the culture volume was replaced at each time point due to sampling). When biosynthesis of target aromatics from glucose in industrial microorganisms, glucose ($C_6H_{12}O_6$) was mainly used for the products and accumulation of biomass ($C_4H_7O_{1.5}N$) that causes about one-third loss of the carbon atoms to CO_2. Assuming that all carbon atoms in glucose were converted into products, biomass and CO_2, by a back-of-the-envelope calculation, the minimum carbon emission during traditional biosynthesis, EC_{TB}, of a target chemical can be calculated as follows: $EC_{TB} = 2 \times (C_{Glucose} - C_{Product} \times N_{Product/Glucose}) \times M_{CO_2}/C_{Product}/M_{Product}$, where $C_{Glucose}$ and $C_{Product}$ are the molar concentrations of consumed glucose and generated product, respectively, $N_{Procuct/Glucose}$ is the number of carbon atoms in the product divided by the number of carbon atoms in glucose (six), and M_{CO_2} and $M_{Product}$ are the molecular weights of CO_2 and the product, respectively. By a back-of-the-envelope calculation, the minimum carbon emission based on the iPRCC strategy, $EC_{iPRCC\text{-}O}$, for α-olefins can be calculated as follows: $EC_{iPRCC\text{-}O} = -(W_{CB\text{-}P} \times C_C \times M_{CO_2}/M_C \times V_P + W_{CA} \times M_{CO_2}/M_{Procuct} \times V_P + W_{CB\text{-}R} \times C_C \times M_{CO_2}/M_C \times V_F)/T_{Product}$, where V_P and V_F are the volume of the carbon sequestration module in the photobioreactor and the volume of the cellular catalysis module in the fermenter, respectively, and $T_{Product}$ is the titre of the product. $W_{CB\text{-}P}$ and $W_{CB\text{-}R}$ refer as the biomass of carbon sequestration module and photosynthetic catalysis module, respectively. $M_C = 12$. The minimum carbon emission based on the iPRCC strategy, EC_{iPRCC}, for other products can be calculated as follows: $EC_{iPRCC} = -(W_{CB\text{-}P} \times C_C \times M_{CO_2}/M_C \times V_P + W_{CA} \times M_{CO_2}/M_{Mediator} \times V_P - W_{CB\text{-}R} \times C_{CE} \times M_{CO_2}/M_C \times V_F)/T_{Product}$. C_{CE} indicates the carbon content of emitted CO_2 (two molecules of carbon per $C_4H_7O_{1.5}N$) for the accumulation of *E. coli* biomass ($C_4H_7O_{1.5}N$, M = 93): (12 × 2)/93. $M_{Mediator}$ indicates the molecular weight of mediator chemical. The positive and negative values of EC indicate the net emission and net absorption of CO_2, respectively.

Reporting summary

Further information on research design is available in the Nature Portfolio Reporting Summary linked to this article.

Data availability

The data supporting the findings of the study are available in the paper and its Supplementary Information. Source data are provided with this paper.

References

1. Wu, C. et al. Acetyl-CoA synthesis through a bicyclic carbon-fixing pathway in gas-fermenting bacteria. *Nat. Synth.* **1**, 615–625 (2022).
2. Cai, T. et al. Cell-free chemoenzymatic starch synthesis from carbon dioxide. *Science* **373**, 1523–1527 (2021).
3. Luo, S. et al. A cell-free self-replenishing CO_2-fixing system. *Nat. Catal.* **5**, 154–162 (2022).
4. Cobb, S. J. et al. Fast CO_2 hydration kinetics impair heterogeneous but improve enzymatic CO_2 reduction catalysis. *Nat. Chem.* **14**, 417–424 (2022).
5. Liu, Y. et al. Biofuels for a sustainable future. *Cell* **184**, 1636–1647 (2021).
6. Jester, B. W. et al. Development of spirulina for the manufacture and oral delivery of protein therapeutics. *Nat. Biotechnol.* **40**, 956–964 (2022).
7. Jiang, W. et al. Metabolic engineering strategies to enable microbial utilization of C1 feedstocks. *Nat. Chem. Biol.* **17**, 845–855 (2021).
8. Miller, T. E. et al. Light-powered CO_2 fixation in a chloroplast mimic with natural and synthetic parts. *Science* **368**, 649–654 (2020).
9. Jaiswal, D., Sahasrabuddhe, D. & Wangikar, P. P. Cyanobacteria as cell factories: the roles of host and pathway engineering and translational research. *Curr. Opin. Biotechnol.* **73**, 314–322 (2022).
10. Wang, X. et al. Enhanced limonene production in cyanobacteria reveals photosynthesis limitations. *Proc. Natl Acad. Sci. USA* **113**, 14225–14230 (2016).
11. Liu, X., Miao, R., Lindberg, P. & Lindblad, P. Modular engineering for efficient photosynthetic biosynthesis of 1-butanol from CO_2 in cyanobacteria. *Energy Environ. Sci.* **12**, 2765–2777 (2019).
12. Yunus, I. S. et al. Synthetic metabolic pathways for conversion of CO_2 into secreted short-to-medium-chain hydrocarbons using cyanobacteria. *Metab. Eng.* **72**, 14–23 (2022).
13. Behler, J., Vijay, D., Hess, W. R. & Akhtar, M. K. CRISPR-based technologies for metabolic engineering in cyanobacteria. *Trends Biotechnol.* **36**, 996–1010 (2018).
14. Richardson, K. N., Black, W. B. & Li, H. Aldehyde production in crude lysate- and whole cell-based biotransformation using a noncanonical redox cofactor system. *ACS Catal.* **10**, 8898–8903 (2020).
15. Kunjapur, A. M., Tarasova, Y. & Prather, K. L. Synthesis and accumulation of aromatic aldehydes in an engineered strain of *Escherichia coli*. *J. Am. Chem. Soc.* **136**, 11644–11654 (2014).
16. Zuñiga, C. et al. Synthetic microbial communities of heterotrophs and phototrophs facilitate sustainable growth. *Nat. Commun.* **11**, 3803 (2020).
17. Wang, L. et al. Engineering consortia by polymeric microbial swarmbots. *Nat. Commun.* **13**, 3879 (2022).
18. Li, T. et al. Mimicking lichens: incorporation of yeast strains together with sucrose-secreting cyanobacteria improves survival, growth, ROS removal, and lipid production in a stable mutualistic co-culture production platform. *Biotechnol. Biofuels* **10**, 55 (2017).
19. Ducat, D. C., Avelar-Rivas, J. A., Way, J. C. & Silver, P. A. Rerouting carbon flux to enhance photosynthetic productivity. *Appl. Environ. Microbiol.* **78**, 2660–2668 (2012).
20. Srinivasan, P. & Smolke, C. D. Biosynthesis of medicinal tropane alkaloids in yeast. *Nature* **585**, 614–619 (2020).
21. Jamieson, C. S., Misa, J., Tang, Y. & Billingsley, J. M. Biosynthesis and synthetic biology of psychoactive natural products. *Chem. Soc. Rev.* **50**, 6950–7008 (2021).
22. Qin, J. et al. Engineering yeast metabolism for the discovery and production of polyamines and polyamine analogues. *Nat. Catal.* **4**, 498–509 (2021).
23. Chen, R. et al. Engineering cofactor supply and recycling to drive phenolic acid biosynthesis in yeast. *Nat. Chem. Biol.* **18**, 520–529 (2022).
24. Ni, J., Wu, Y. T., Tao, F., Peng, Y. & Xu, P. A coenzyme-free biocatalyst for the value-added utilization of lignin-derived aromatics. *J. Am. Chem. Soc.* **140**, 16001–16005 (2018).
25. Ni, J., Gao, Y. Y., Tao, F., Liu, H. Y. & Xu, P. Temperature-directed biocatalysis for the sustainable production of aromatic aldehydes or alcohols. *Angew. Chem. Int. Ed.* **57**, 1214–1217 (2018).
26. Kim, S. I. et al. Cu(I)-incorporation strategy for developing styrene selective adsorbents. *Chem. Eng. J.* **425**, 130601 (2021).
27. Grubbe, W. S., Rasor, B. J., Krüger, A., Jewett, M. C. & Karim, A. S. Cell-free styrene biosynthesis at high titers. *Metab. Eng.* **61**, 89–95 (2020).
28. Nagy, E. Z. et al. Mapping the hydrophobic substrate binding site of phenylalanine ammonia-lyase from *Petroselinum crispum*. *ACS Catal.* **9**, 8825–8834 (2019).

29. Ni, J. et al. Remodeling of the photosynthetic chain promotes direct CO_2 conversion into valuable aromatic compounds. *Angew. Chem. Int. Ed.* **57**, 15990–15994 (2018).
30. Yang, D., Park, S. Y., Park, Y. S., Eun, H. & Lee, S. Y. Metabolic engineering of *Escherichia coli* for natural product biosynthesis. *Trends Biotechnol.* **38**, 745–765 (2020).
31. Yang, D., Jang, W. D. & Lee, S. Y. Production of carminic acid by metabolically engineered *Escherichia coli*. *J. Am. Chem. Soc.* **143**, 5364–5377 (2021).
32. Liu, Q., Liu, Y., Chen, Y. & Nielsen, J. Current state of aromatics production using yeast: achievements and challenges. *Curr. Opin. Biotechnol.* **65**, 65–74 (2020).
33. Abramson, B. W., Kachel, B., Kramer, D. M. & Ducat, D. C. Increased photochemical efficiency in cyanobacteria via an engineered sucrose sink. *Plant Cell Physiol.* **57**, 2451–2460 (2016).
34. Santos-Merino, M. et al. Improved photosynthetic capacity and photosystem I oxidation via heterologous metabolism engineering in cyanobacteria. *Proc. Natl Acad. Sci. USA* **118**, e2021523118 (2021).
35. Singh, A. K., Santos-Merino, M., Sakkos, J. K., Walker, B. J. & Ducat, D. C. Rubisco regulation in response to altered carbon status in the cyanobacterium *Synechococcus elongatus* PCC 7942. *Plant Physiol.* **189**, 874–888 (2022).
36. Dann, M. et al. Enhancing photosynthesis at high light levels by adaptive laboratory evolution. *Nat. Plants* **7**, 681–695 (2021).
37. Hill, N. C., Tay, J. W., Altus, S., Bortz, D. M. & Cameron, J. C. Life cycle of a cyanobacterial carboxysome. *Sci. Adv.* **6**, eaba1269 (2020).
38. Cameron, J. C., Wilson, S. C., Bernstein, S. L. & Kerfeld, C. A. Biogenesis of a bacterial organelle: the carboxysome assembly pathway. *Cell* **155**, 1131–1140 (2013).
39. Luan, G., Zhang, S., Wang, M. & Lu, X. Progress and perspective on cyanobacterial glycogen metabolism engineering. *Biotechnol. Adv.* **37**, 771–786 (2019).
40. Payne, K. A. et al. New cofactor supports α,β-unsaturated acid decarboxylation via 1,3-dipolar cycloaddition. *Nature* **522**, 497–501 (2015).
41. Liu, C. et al. A systematic optimization of styrene biosynthesis in *Escherichia coli* BL21 (DE3). *Biotechnol. Biofuels* **11**, 14 (2018).
42. Erickson, E. et al. Critical enzyme reactions in aromatic catabolism for microbial lignin conversion. *Nat. Catal.* **5**, 86–98 (2022).
43. Liu, Z., Wang, K., Chen, Y., Tan, T. & Nielsen, J. Third-generation biorefineries as the means to produce fuels and chemicals from CO_2. *Nat. Catal.* **3**, 274–288 (2020).
44. Aleku, G. A. et al. Enzymatic C–H activation of aromatic compounds through CO_2 fixation. *Nat. Chem. Biol.* **16**, 1255–1260 (2020).
45. Palmer, C. M., Miller, K. K., Nguyen, A. & Alper, H. S. Engineering 4-coumaroyl-CoA derived polyketide production in *Yarrowia lipolytica* through a β-oxidation mediated strategy. *Metab. Eng.* **57**, 174–181 (2020).
46. Kummer, M. J. et al. Substrate channeling by a rationally designed fusion protein in a biocatalytic cascade. *JACS Au* **1**, 1187–1197 (2021).
47. Lin, J. L., Palomec, L. & Wheeldon, I. Design and analysis of enhanced catalysis in scaffolded multienzyme cascade reactions. *ACS Catal.* **4**, 505–511 (2014).
48. Brey, L. F. et al. Metabolic engineering of *Synechocystis* sp. PCC 6803 for the production of aromatic amino acids and derived phenylpropanoids. *Metab. Eng.* **57**, 129–139 (2020).
49. Ni, J., Tao, F., Wang, Y., Yao, F. & Xu, P. A photoautotrophic platform for the sustainable production of valuable plant natural products from CO_2. *Green Chem.* **18**, 3537–3548 (2016).
50. Hu, G. et al. Light-driven CO_2 sequestration in *Escherichia coli* to achieve theoretical yield of chemicals. *Nat. Catal.* **4**, 395–406 (2021).
51. Gao, H. et al. Applications of synthetic light-driven microbial consortia for biochemicals production. *Bioresour. Technol.* **351**, 126954 (2022).
52. Li, T. et al. Creating a synthetic lichen: mutualistic co-culture of fungi and extracellular polysaccharide-secreting cyanobacterium *Nostoc* PCC 7413. *Algal Res.* **45**, 101755 (2020).
53. Li, C. et al. A highly compatible phototrophic community for carbon-negative biosynthesis. *Angew. Chem. Int. Ed.* **62**, e202215013 (2023).
54. Santos-Merino, M., Yun, L. & Ducat, D. C. Cyanobacteria as cell factories for the photosynthetic production of sucrose. *Front. Microbiol.* **14**, 1126032 (2023).
55. Yuan, Y. et al. Efficient exploration of terpenoid biosynthetic gene clusters in filamentous fungi. *Nat. Catal.* **5**, 277–287 (2022).
56. Zahedipour, F. et al. Potential effects of curcumin in the treatment of COVID-19 infection. *Phytother. Res.* **34**, 2911–2920 (2020).
57. Sundaram, S. et al. A modular in vitro platform for the production of terpenes and polyketides from CO_2. *Angew. Chem. Int. Ed.* **60**, 16420–16425 (2021).
58. Haider, T. P., Völker, C., Kramm, J., Landfester, K. & Wurm, F. R. Plastics of the future? The impact of biodegradable polymers on the environment and on society. *Angew. Chem. Int. Ed.* **58**, 50–62 (2019).
59. Weiss, T. L., Young, E. J. & Ducat, D. C. A synthetic, light-driven consortium of cyanobacteria and heterotrophic bacteria enables stable polyhydroxybutyrate production. *Metab. Eng.* **44**, 236–245 (2017).
60. Long, B. et al. Machine learning-informed and synthetic biology-enabled semi-continuous algal cultivation to unleash renewable fuel productivity. *Nat. Commun.* **13**, 541 (2022).
61. Mildenberger, M., Lachapelle, E., Harrison, K. & Stadelmann-Steffen, I. Limited impacts of carbon tax rebate programmes on public support for carbon pricing. *Nat. Clim. Change* **12**, 141–147 (2022).

Acknowledgements

This work was supported by the National Natural Science Foundation of China (grant no. 32071418 to J.N.), the National Key Research and Development Program of China (grant no. 2019YFA0904603 to J.N.) and the Shanghai Rising-Star Program (grant no. 20QA1404800 to J.N.). We are grateful to the High-Performance Computing Platform and Y-BioFoundry of LumyBio. We also thank D. Yan for language polishing this paper.

Author contributions

J.N. conceived the project and supervised the research. C.L., L.Y. and H.Z. performed the experiments and analysed the data. J.W. performed the in silico analysis. J.N. and C.L. wrote the manuscript with contributions from and discussions with all the authors.

Competing interests

The authors declare no competing interests.

Additional information

Supplementary information The online version contains supplementary material available at https://doi.org/10.1038/s44160-023-00331-5.

Correspondence and requests for materials should be addressed to Jun Ni.

Peer review information *Nature Synthesis* thanks Rodrigo Ledesma-Amaro, Lennart Schada von Borzyskowski and Elton Hudson for their contribution to the peer review of this work. Primary Handling Editor: Thomas West, in collaboration with the *Nature Synthesis* team.

nature portfolio

Corresponding author(s): DBPR NATSYNTH-22090985

Last updated by author(s): Mar 13, 2023

Reporting Summary

Nature Portfolio wishes to improve the reproducibility of the work that we publish. This form provides structure for consistency and transparency in reporting. For further information on Nature Portfolio policies, see our Editorial Policies and the Editorial Policy Checklist.

Statistics

For all statistical analyses, confirm that the following items are present in the figure legend, table legend, main text, or Methods section.

n/a	Confirmed
☐	☒ The exact sample size (*n*) for each experimental group/condition, given as a discrete number and unit of measurement
☐	☒ A statement on whether measurements were taken from distinct samples or whether the same sample was measured repeatedly
☒	☐ The statistical test(s) used AND whether they are one- or two-sided *Only common tests should be described solely by name; describe more complex techniques in the Methods section.*
☒	☐ A description of all covariates tested
☒	☐ A description of any assumptions or corrections, such as tests of normality and adjustment for multiple comparisons
☐	☒ A full description of the statistical parameters including central tendency (e.g. means) or other basic estimates (e.g. regression coefficient) AND variation (e.g. standard deviation) or associated estimates of uncertainty (e.g. confidence intervals)
☒	☐ For null hypothesis testing, the test statistic (e.g. *F*, *t*, *r*) with confidence intervals, effect sizes, degrees of freedom and *P* value noted *Give P values as exact values whenever suitable.*
☒	☐ For Bayesian analysis, information on the choice of priors and Markov chain Monte Carlo settings
☒	☐ For hierarchical and complex designs, identification of the appropriate level for tests and full reporting of outcomes
☒	☐ Estimates of effect sizes (e.g. Cohen's *d*, Pearson's *r*), indicating how they were calculated

Our web collection on statistics for biologists contains articles on many of the points above.

Software and code

Policy information about availability of computer code

Data collection	Agilent OpenLab CDS 2.6; BGISEQ-500 platform; Tecan FluentControl, SparkControl 3.2
Data analysis	Agilent OpenLab CDS 2.6; OriginPro 2018C; Microsoft Excel 2208; ParaFold; Bowtie2 v2.2.5; RSEM v1.2.12; Pymol 2.5.2; Caver 3.0

For manuscripts utilizing custom algorithms or software that are central to the research but not yet described in published literature, software must be made available to editors and reviewers. We strongly encourage code deposition in a community repository (e.g. GitHub). See the Nature Portfolio guidelines for submitting code & software for further information.

Data

Policy information about availability of data

All manuscripts must include a data availability statement. This statement should provide the following information, where applicable:

- Accession codes, unique identifiers, or web links for publicly available datasets
- A description of any restrictions on data availability
- For clinical datasets or third party data, please ensure that the statement adheres to our policy

The authors declare that all data supporting the findings of this study are available within this paper and its supplementary files.

Human research participants

Policy information about studies involving human research participants and Sex and Gender in Research.

Reporting on sex and gender	N/A
Population characteristics	N/A
Recruitment	N/A
Ethics oversight	N/A

Note that full information on the approval of the study protocol must also be provided in the manuscript.

Field-specific reporting

Please select the one below that is the best fit for your research. If you are not sure, read the appropriate sections before making your selection.

☒ Life sciences ☐ Behavioural & social sciences ☐ Ecological, evolutionary & environmental sciences

For a reference copy of the document with all sections, see nature.com/documents/nr-reporting-summary-flat.pdf

Life sciences study design

All studies must disclose on these points even when the disclosure is negative.

Sample size	No sample size calculation was performed. Sample size and experimental replicates were chosen based on previous experience and literature reports in the field.
Data exclusions	No data were excluded from the analyses.
Replication	Each experiment was reproduced at least three times independently. All attempts at replication were successful.
Randomization	N/A
Blinding	N/A

Reporting for specific materials, systems and methods

We require information from authors about some types of materials, experimental systems and methods used in many studies. Here, indicate whether each material, system or method listed is relevant to your study. If you are not sure if a list item applies to your research, read the appropriate section before selecting a response.

Materials & experimental systems

n/a	Involved in the study
☒	☐ Antibodies
☒	☐ Eukaryotic cell lines
☒	☐ Palaeontology and archaeology
☒	☐ Animals and other organisms
☒	☐ Clinical data
☒	☐ Dual use research of concern

Methods

n/a	Involved in the study
☒	☐ ChIP-seq
☒	☐ Flow cytometry
☒	☐ MRI-based neuroimaging